

LARGE EDDY SIMULATIONS OF THE FLOW AROUND A SQUARE CYLINDER

Germán Filippini*, Gerardo Franck*,
Norberto Nigro*, Mario Storti* and Jorge D'Elía*

*Centro Internacional de Métodos Computacionales en Ingeniería (CIMEC)
Instituto de Desarrollo Tecnológico para la Industria Química (INTEC)
Universidad Nacional del Litoral - CONICET
Parque Tecnológico Litoral Centro (PTLC) s/n, 3000-Santa Fe, Argentina
e-mail: gfilippini@ceride.gov.ar, (gfranck,nnigro,mstorti,jdelia)@intec.unl.edu.ar
web page: <http://venus.ceride.gov.ar/CIMEC>

Key Words: bluff bodies, wake flow, turbulence, large eddy simulation, finite elements, parallel computing, fluid mechanics

Abstract.

Large Eddy Simulations (LES) of the three-dimensional flow around fixed bluff bodies have been performed in two benchmarks: a square cylinder (case A) and a wall-mounted cube (case B), as denoted by Rodi et al. (ASME transaction, vol. 119, pp. 248-262, June 1997). Due to some differences in the flow modeling, in this communication case A is considered while in a companion work the results for the other case are shown. In case A, the flow around a square cylinder, experiments show a typical unsteady-flow regime with a periodic wake (the von Kármán vortex street) although there is some modulation on the periodicity. The selected flow conditions for the present numerical simulations are taken from those suggested by Rodi et al. Time-averaged and instantaneous flow visualizations are used to clarify the flow behavior and are then contrasted to the experiment ones.

1 INTRODUCTION

1.1 Unsteady turbulent flows around bluff bodies

Unsteady separated flows around bluff bodies such as cubes, rectangular and circular cylinders, and flat plates are relevant to many engineering designs, such as constructions under the action of wind loading like buildings, chimneys and water tank towers, steel tower suspension bridges or marine structures under the action of water loading.

For numerical validations, some test cases have been chosen as benchmarks in the turbulence modeling community where several numerical methods, Sub-Grid Stress (SGS) models and mesh resolutions are currently validated (e.g. see Kogaki et al., Fluid Dynamics Research, vol. 20, pp. 11-24, 1997). Guidelines for the selection of LES test cases performed in the Rottach-Egem (RE-1995) Workshop¹ (Germany, 26-28 June, 1995) were, among others, the following:

- The Reynolds number should be high enough to be out of reach of a Direct Numerical Simulation (DNS) of turbulence but not so high that the model is the dominant factor in the simulation;
- The geometry should be complicated enough to render DNS unfeasible but not so complicated that the number of grid points needed for an accurate representation of the geometry is relatively too high;
- The physics of the flow should be relatively intricate. At least, the flow should have significant secondary flow separation and other “extra strains” making the Reynolds averaged modeling difficult;
- Reliable and complete experimental measurement of the flow should be available;
- The bodies geometries should be relatively easy for gridding. In particular, bodies geometries that can be treated with a Cartesian coordinate system.

In the RE-1995 workshop, among other benchmarks, two cases were proposed: a *square cylinder (case A)* and a *wall-mounted cube (case B)*, as denoted by Rodi et al. Both benchmarks are oriented to the flow around bluff-bodies, and they are suitable to explore the feasibility of the LES to related engineering problems because they show complicated flow events such as massive separations, impinging, transition to turbulence and formation of vortex streets.

A basic difference between cases A and B in the present numerical simulations is related to the incoming flow: in the square cylinder (case A) a piston-flow is assumed in the inflow section, so the turbulence is only generated by the cylinder surfaces, while in the wall-mounted cube (case B), a “precursor” computation is performed. In the “precursor” approach, following the Sagaut taxonomy², a previous computation is done

for the attached boundary layer flow without the body, and then an extraction plane is defined whose data is used as an inlet boundary condition.

A reason for a focus on LES for modeling the flow around bluff bodies is related to the rather poor results when using Reynolds Average Navier-Stokes (RANS) equations based on the statistical turbulent models. Most probably this has to do with complicating factors such as massive flow separation, streamline curvature, transition from laminar to turbulent regime, recirculation, vortex shedding and perhaps, the most relevant one, the existence of inherent three dimensional flow structures^{3,4}.

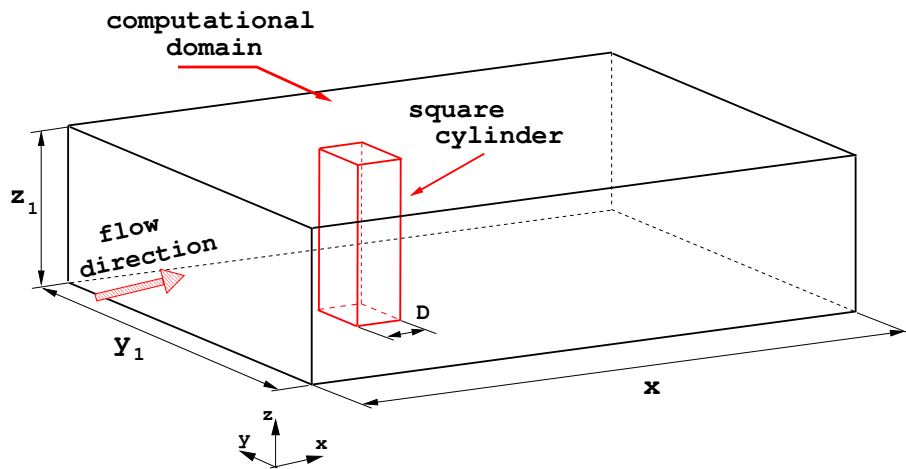


Figure 1: Sketch for the square cylinder flow test.

1.2 Some laboratory facts

The benchmark *case A* of the RE-1995 workshop is the flow over the *square cylinder*, see Fig. 1. The laboratory experiments of Lyn^{5,6} *et al.* were performed using a Laser Doppler velocimeter for a bulk Reynolds number of 22 000, the inflow was reported to have a turbulence level of 2 percent at 4.5 cylinders widths upstream from the cylinder, although no length scale data was given for this turbulence. It was reported that the separation and the wake were periodic although there was some modulation of the periodicity. In addition to time-average quantities some phase-average ones, at various flow locations, were also given. Some flow-visualizations techniques were employed, like oil-films. Unfortunately, the region near the cylinder walls was not resolved in the measurements, so the number and type of vortices could not be given.

1.3 The CFD-benchmark

The flow-domain for this benchmark is a parallelepiped that has $20.5 D \times 14 D \times 4 D$ in the streamwise x , spanwise y and stream-normal (vertical) z Cartesian directions and is summarized in Table 1. The bulk Reynolds (based on the cylinder diameter) was fixed in

22 000, while the suggested boundary conditions in the RE-1995 workshop were:

1. Free-slip (symmetry) on the upper and lower surface as well as the lateral boundaries of the computational flow domain;
2. A choice of zero gradient or convective boundary conditions at the outflow boundary;
3. A choice of no-slip boundary condition or wall functions at the cylinder surface;
4. However, the inflow condition was not clearly specified. Although the inflow conditions in the laboratory experiments^{5,6} *et al.* were reported to contain about 2 % of relative turbulence intensity, the sixteen CFD-simulations presented in the RE-1995 workshop assumed, in fact, an uniform inflow condition.

It was also suggested in the RE-1995 workshop that a sufficiently fine grid should be used for a better resolution of the near-wall flow in case of no-slip boundary conditions. On the other hand, from a critical review of the presented CFD simulations, it was concluded that an accurate prediction of the Strouhal number is not necessarily an indicator of a quality simulation since this adimensional number is not too sensitive to the simulation parameters.

1.4 Main objectives of this work

The purpose of this work is to perform the benchmark *case A* of the RE-1995 workshop, i.e. the flow around the *square cylinder*, as a calibration of the employed CFD-FEM solver for later use in turbulent flows over bluff bodies from an engineering perspective. The bulk Reynolds (based on the cylinder diameter) is fixed in 22 000, while the selected boundary conditions are the following: a piston flow at the inlet, no-slip condition at the wall-surface of the cylinder, free-slip on the upper and lower surface as well as lateral boundaries, while at the outflow boundary a free-traction is assumed. An unsteady flow of an incompressible viscous fluid of Newtonian type is assumed in the numerical simulations, and it is modeled by a Large Eddy Simulation (LES) paradigm together with the standard Smagorinsky model, as Subgrid Scale Modeling (SGM), and the van Driest near-wall damping. A monolithic computational code is employed, which is based on stabilized finite elements by means of a Streamline Upwind Petrov Galerkin (SUPG) and Pressure Stabilized Petrov Galerkin (PSPG) composed scheme. Parallel computing on a Beowulf cluster with a decomposition domain technique is used. An unstructured grid with non-uniform resolution is selected. Visualization of the time-averaged flow in the near-wake include: (i) streamlines; (ii) velocity planes; and (iii) isosurfaces of pressure and surface. The time average velocities and turbulent stresses are computed and compared with the experiments of Lyn^{5,6} *et al.* and Martinuzzi-Tropea⁷.

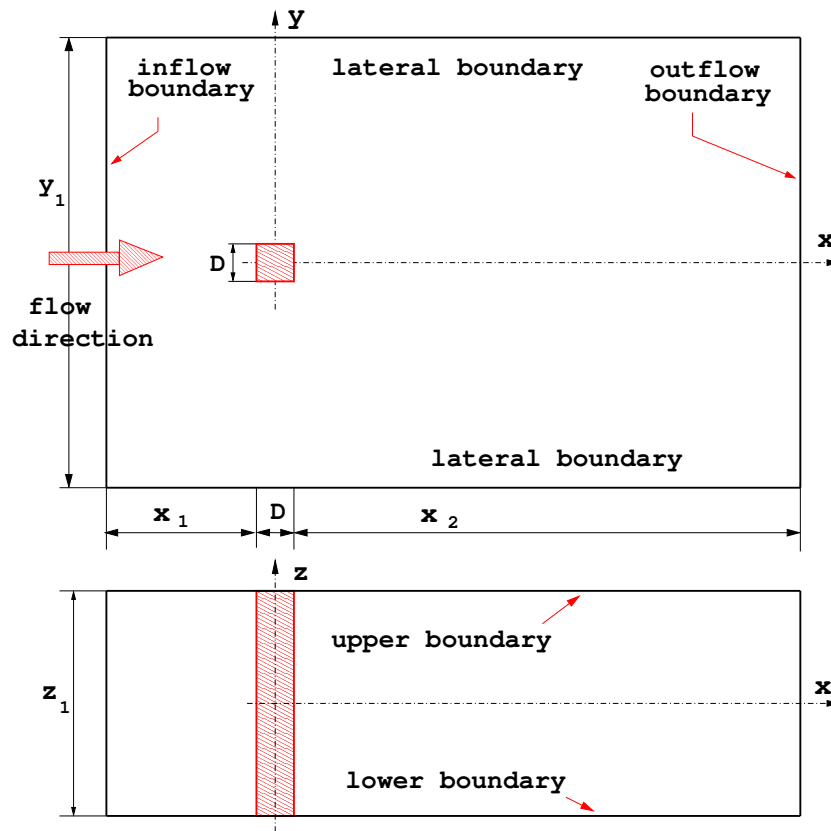


Figure 2: Definition of the computational flow-domain for the square cylinder flow.

2 COMPUTATIONAL PARAMETERS

2.1 Geometrical parameters

Figs. 2 and 1 show the relative dimensions of the computational flow domain. A Cartesian coordinate system $O(x, y, z)$ is employed whose origin is placed on the ground. The square cylinder is placed between $x = -0.5$ and $x = 0.5$ which side is $D = 1$ and its height is $H = 4 D$. The flow-domain is a parallelepiped that has $20.5 D \times 14 D \times 4 D$ in the streamwise x , spanwise y and stream-normal (vertical) z Cartesian directions and is summarized in Table 1. The inlet flow section is placed to $x_1 = 4.5 D$ upstream with respect to the body front while the outlet flow section is placed to $x_2 = 15 D$ downstream from the body rear-end.

x_1/D	x_2/D	y_1/D	z_1/D
4.5	15	14	4

Table 1: Dimensions of the computational flow-domain for the square cylinder flow.

2.2 Fluid and flow parameters

A Newtonian viscous fluid model is assumed and kinematic viscosity ν . The bulk Reynolds number is $Re = U_b D / \nu = 22\,000$, based on the bulk speed $U_b = \langle U \rangle_\Omega$ and the cylinder side is $D = 1$.

2.3 Boundary conditions and time step

The selected boundary conditions in the present numerical simulations are the following: (i) piston flow profile $\mathbf{U}_b(\mathbf{x}, t)$ at inlet; (ii) no-slip at the ground and upper surface; (iii) null pressure at outlet; (iv) no-slip at the body surface ($\mathbf{u} = \mathbf{0}$) and (v) slip at the lateral sides. At the entrance to the flow domain a uniform flow is imposed (no-perturbation is added). The size of the time-step was selected as $\Delta t = 0.05$ s, while the statistics were computed after the flow was sufficiently developed.

3 NUMERICAL SCHEME

3.1 Finite element mesh

An unstructured tetrahedral grid with $nel = 1\,504\,K$ – elements and $nod = 266\,K$ – nodes is employed. The mesh has a non-uniform resolution, where the grid-space is stretched near the square cylinder. The body surface has $nel_{sup} = 103\,K$ – elements (triangular planar). Fig. 3 shows a xz -cut at the vertical plane (at the vertical middle section of the flow-domain), and Fig. 4 shows a xy -cut at the horizontal plane (at the horizontal middle section), around the square cylinder. Finally, Fig. 5 shows a perspective view of the mesh close to the square cylinder.

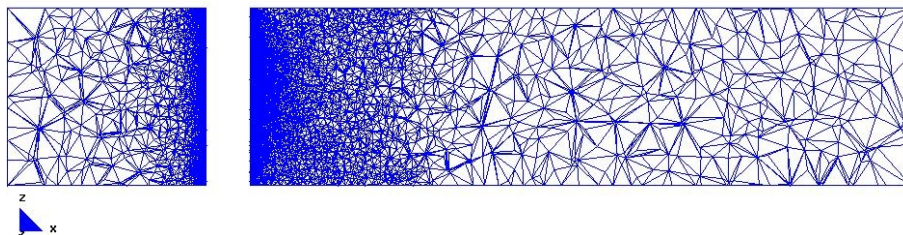


Figure 3: Vertical xz -cut of the unstructured finite element mesh around the square cylinder.

3.2 SUPG-PSPG finite element solver

The numerical simulations are performed by a stabilized finite element scheme for the unsteady Navier-Stokes (NS) equations where, at each node and at each time step, the momentum and continuity equations are solved for the three components of velocity and pressure. The combined Streamline Upwind Petrov Galerkin (SUPG) and Pressure Stabilized Petrov Galerkin (PSPG) scheme, proposed by Tezduyar⁸ *et al.* is employed for stabilization of the advection and incompressibility terms.

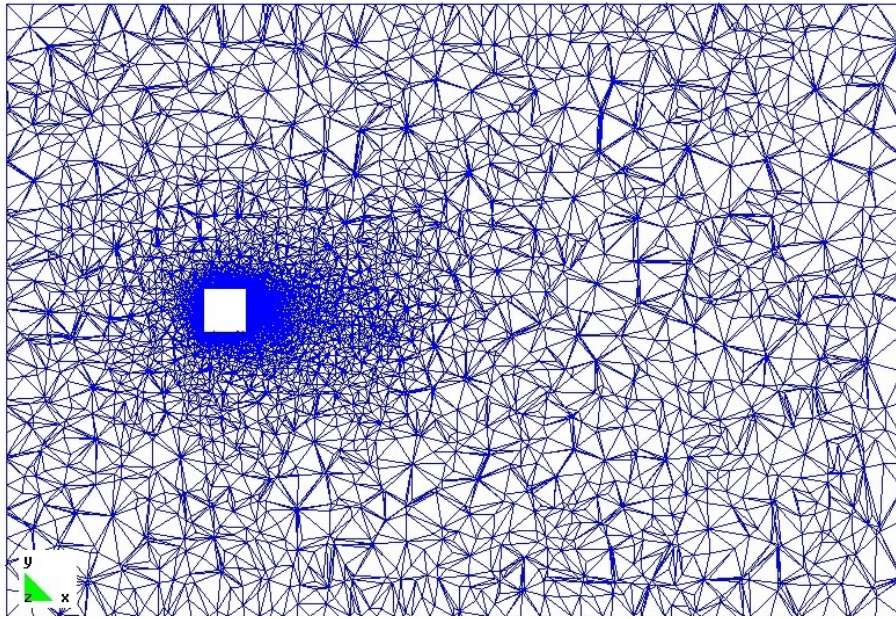


Figure 4: Horizontal xy -cut of the unstructured finite element mesh around the square cylinder.

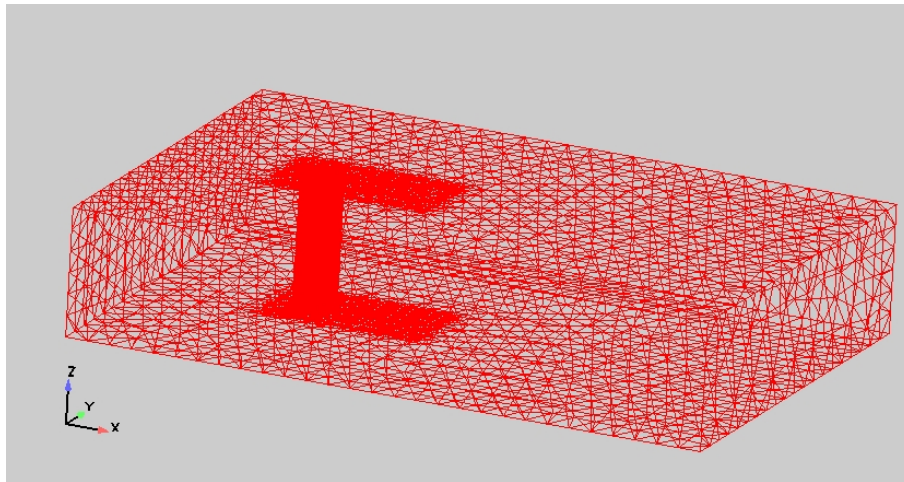


Figure 5: Perspective view of the unstructured finite element mesh around the square cylinder.

3.3 Large Eddy Simulation (LES)

The computational code solves the momentum balance equations with an “effective” kinematic viscosity $\nu_e = \nu_n + \nu_t$, which is the sum of the molecular ν viscosity plus the “turbulent” one ν_t . The latter one is estimated by means of the Smagorinsky⁹ sub-grid model

with van Driest near-wall damping and given by

$$\begin{aligned}\nu_t &= C_S^2 h_e^2 f_\nu \sqrt{\epsilon(\mathbf{u}) : \epsilon(\mathbf{u})} ; \\ f_\nu &= 1 - \exp(-y^+/A^+) ;\end{aligned}\tag{1}$$

in which C_S is the Smagorinsky constant ($C_S \approx 0.10$ for flows in ducts), h_e is a typical element diameter and $\epsilon(u) : \epsilon(u)$ is the trace of the strain rate $\epsilon(u)$. The van Driest near-wall damping f_ν reduces the “turbulent” kinematic viscosity close to the solid walls, and it introduces non-localities in the sense that the “turbulent” kinematic viscosity ν_t at a volume element depends on the state of the fluid at a wall, a constant value $A^+ = 25$ is adopted, $y^+ = y/y_w$ is the non-dimensional distance from the nearest wall expressed in wall units $y_w = \nu/u_\tau$, $u_\tau = (\tau_w/\rho)^{1/2}$ is the local friction velocity, τ_w is the local wall shear stress and ρ is the fluid density.

3.4 Parallel computing

The numerical simulations are performed by the PETSc-FEM¹⁰ code, which is a parallel multi-physics^{11,12,13} finite element library based on the Message Passing Interface (MPI, <http://www.mpi-forum.org>) and the Portable Extensible Toolkit for Scientific Computations (PETSc, <http://www-fp.mcs.anl.gov/petsc>). Its “Interface Iterative and Sub-domain Direct” (IISDMat) class has been employed¹⁴, which solves the linear system by iteration over the interface nodes while a direct method is employed in each interior sub-domain (this is commonly referred as a *Domain Decomposition Method* (DDM)). The computations were performed in the CIMEC-Beowulf cluster, where the CPU time per each time-step was approximately $t_{step} \approx 5$ minutes.

4 VISUALIZATIONS OF THE NUMERICAL RESULTS

4.1 Some terminology

The following terminology for the computational visualizations will be employed in the next subsections:

1. The *particle-trace* visualizes an instantaneous vector field. It can be (at least) a *line* or a *ribbon*;
2. The particle-trace *line* visualizes an instantaneous vector field by displaying the path that a particle would follow if it were placed in that field. The particle can be chosen with mass or massless. The tangent to a particle-trace line is parallel to the instantaneous vector field at each point;
3. A *stream-line* is the same as a particle-trace line but for a steady-vector field or for an unsteady one at some prescribed time;

4. A *stream-ribbon* is a particle-trace line that additionally visualize the rotation of a vector field around the particle path. This is done through a *ribbon* whose *width* is some user-specified value, while its *twisting* is determined by the rotation of the flow around the particle path;
5. A *surface-restricted* line is one which is constrained at some cut-plane defined by the user, where only the projected vector-field is employed. Its values can be the vector magnitude (with the restriction that it can not be zero) as well as some of its components;
6. Additionally, the term *speed* will be used as abbreviation for the *squared velocity module*.

In some visualization softwares, the particle-trace lines and stream-lines are computed with bar elements, while the stream-ribbon lines consist of 4-noded quadrilaterals with its end-edges parallel to the z -axis of the global frame. At each integration-step of the vector field, the leading edge is rotated around the current direction of the path by the same amount that the vector field has rotated around the path.

4.2 General visualization scheme

The instantaneous-flow behavior will be compared to the time-averaged one in some cases.

The stream-lines and stream-ribbons are used to visualize separations and re-attachments in different places of the flow domain: front, top, bottom and lateral sides of the wind-tunnel, and behind the square cylinder.

The stream-lines are projected onto the vertical xz -symmetric plane ($y = 0$) and the following horizontal xy -planes: (i) at the floor ($z = 0$), near the ground ($z = 0.1 D$) and at the middle cylinder height ($z = 2 D$). A better picture of the flow nature can be obtained from the streamlines of the time-averaged flow at some time-steps of the numerical simulation.

The stream-ribbons are used for a visualization of the flow features in the lateral and near-wakes, while the trace-lines are visualized onto the body surface.

Finally, iso-surfaces and contour-fills of pressure and speed are also used for identifying some coherent structures and quasi-periodic subflows.

4.2.1 At the middle horizontal xy -plane ($z = 2 D$)

Fig. 6 shows some speed trace-lines for the time-averaged flow and the instantaneous one (left and right, respectively). These are streamlines that are projected onto the middle horizontal plane $z = 2 D$ (at the middle cylinder height).

The speed trace-lines of the time-averaged flow show: (i) two recirculation regions with their foci on the lateral sides, and (ii) a pair of vortices with their foci behind the body.

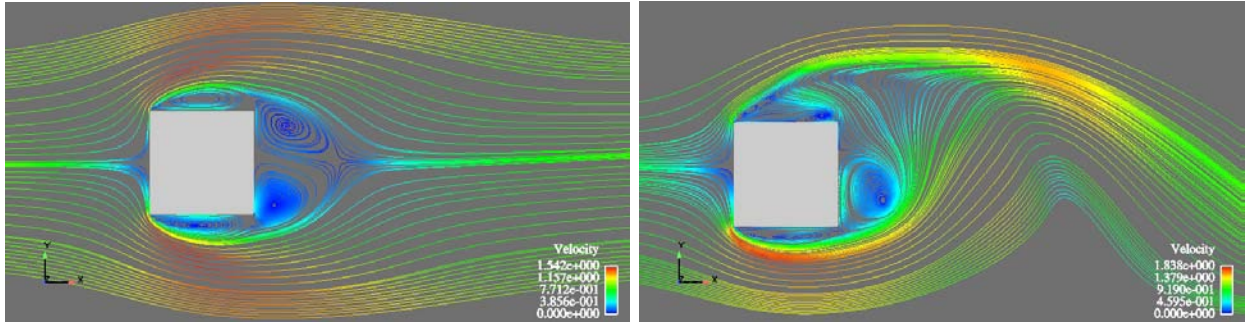


Figure 6: Speed trace-lines over the horizontal xy -plane at $z = 2 D$ (at the middle cylinder height): time-averaged flow (left) and instantaneous one (right).

However, it should be stressed that the vortices pair behind the body that are observed in the time-averaged flow are not seen in the instantaneous one where a recirculation flow is observed instead. This is a difference between both visualizations.

On the other hand, a saddle point downstream the vortices and behind the cylinder is also observed. In the front of the body both pictures show a laminar-like regime with an impact-point followed by a horseshoe vortex.

All vortices, behind the cylinder and on its lateral sides, are visualized using stream-lines colored with the speed.

4.2.2 At the symmetric vertical- xz -plane ($y = 0$)

The flow topology in this plane through the trace-lines for the time-averaged flow (see Fig. 7, left) shows two vortices close to the top and bottom surfaces and close to the separation line in the near-wake. On the other hand, the corresponding ones for the instantaneous-flow (see Fig. 7, right) show several vortices behind the square cylinder, where the multiple vortex system can be visualized using trace-lines projected on the vertical xz -symmetric plane. In Fig. 8 trace-lines and stream-ribbons are shown on the lateral sides. This is

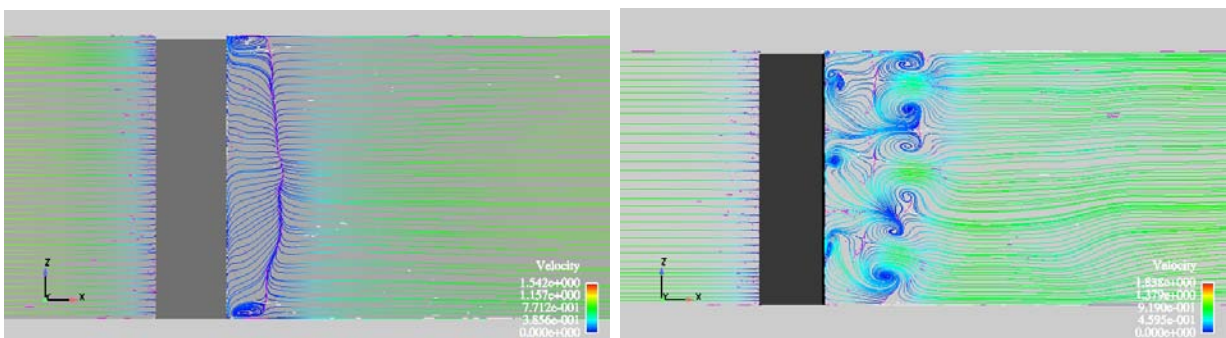


Figure 7: Trace-lines on the vertical symmetrical xz -plane ($y = 0$) for the time-averaged flow (left) and for the instantaneous one (right).

performed for the time-averaged flow (left) as well as for the instantaneous one (right). In both pictures an eigenvalue analysis (e.g. see Perry-Chong¹⁵, Kenwright¹⁶, Hesselink¹⁷) is used for a computation of the vortex cores in the regions that produce recirculating flows (its cores are colored in red).

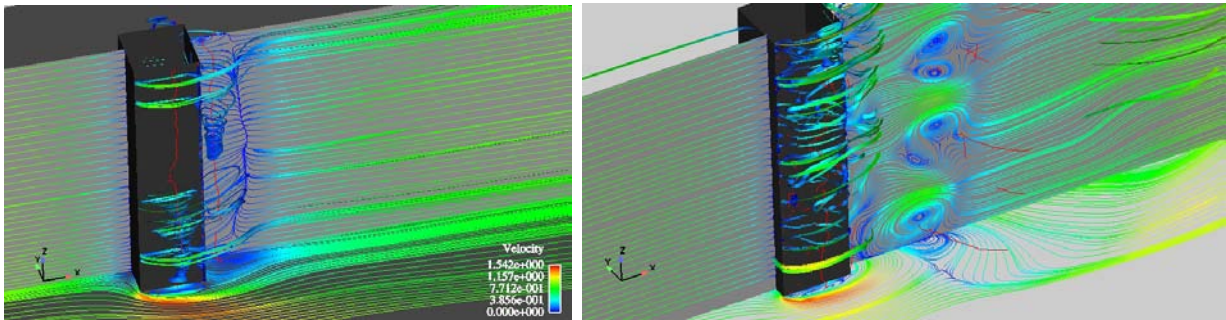


Figure 8: Trace-lines and stream-ribbons at the symmetric vertical xz -plane ($y = 0$), horizontal xy -one and lateral sides: time-averaged flow (left) and instantaneous-one (right). Red lines represent vortex cores.

4.2.3 At the floor-plane ($z = 0$)

The streamlines of the time-averaged flow projected onto the floor plane show evidence of a different behavior with respect to the half-plane, see Fig. 9, left. Two lateral vortices can be observed, but the near-wake (behind the square cylinder) does not show the two recirculation regions like the half-plane. Fig. 9, right, shows that the unsteadiness feature of the flow is visible through the trace-lines for the instantaneous-flow. Fig. 10 shows a

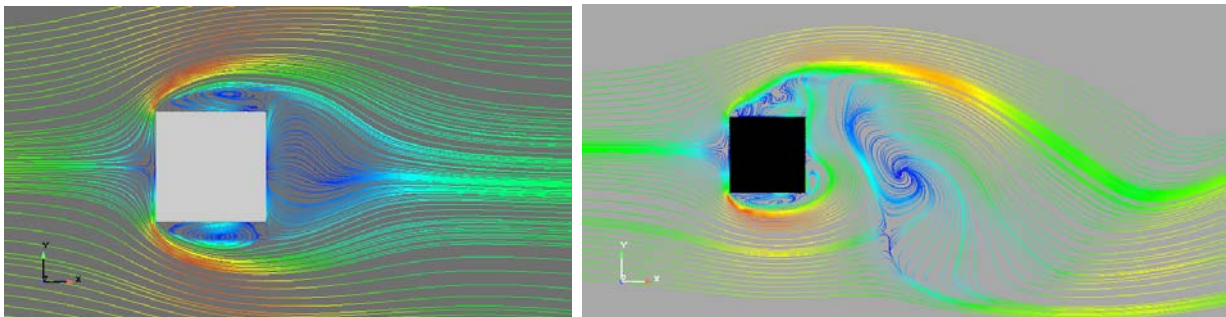


Figure 9: Trace-lines on the floor plane ($z = 0$): time-averaged flow (left) and instantaneous-one (right).

view of the different behavior of the trace-lines for the time-averaged flow on the horizontal planes: at the middle-cylinder height and close to the ground.

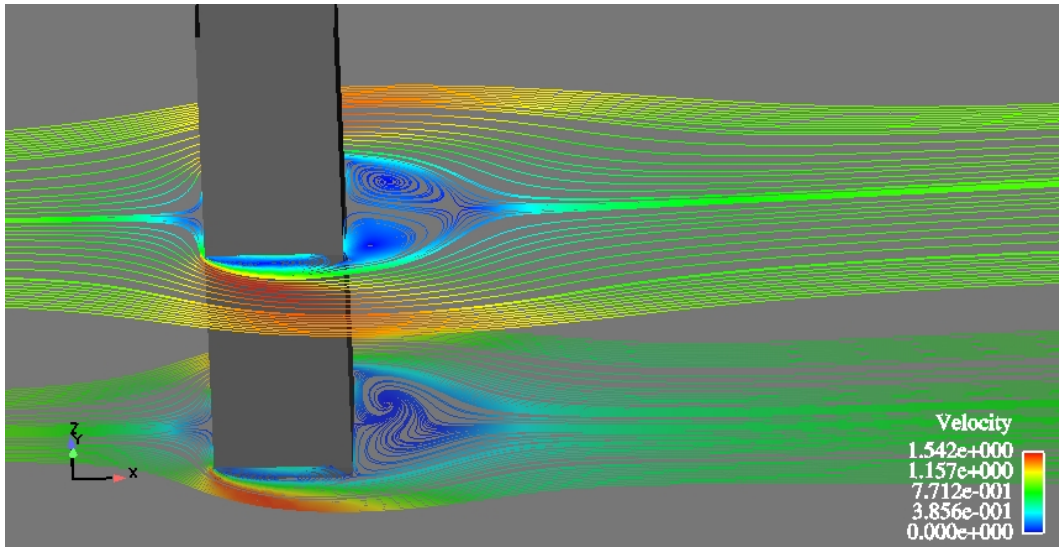


Figure 10: Trace-lines comparison for the time-averaged flow: at the middle-cylinder height and close to the ground.

4.2.4 Stream-ribbons

Stream-ribbons for the time-averaged flow are shown in Fig. 11, where an exchange of fluid between the separation regions can be observed. From this picture it can be concluded that the separation-region around a three-dimensional bluff-body cannot be closed. To support this conclusion, Fig. 12 shows the stream-ribbons at the lateral sides like in the near-wake behind the square cylinder. It can be observed how these stretch from the lateral to the back vortices showing a fluid exchange among the vortices.

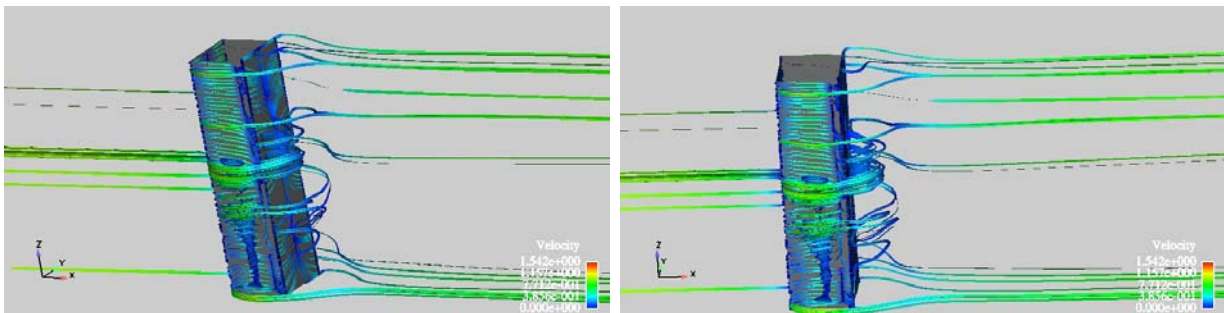


Figure 11: Stream-ribbons for the time-averaged flow: lateral and rear views.

4.2.5 Trace-lines

In Fig.13 trace-lines for the time-averaged flow are plotted on the body surface showing a regular flow in the front face and lateral sides. Lengthwise and in the middle of the back

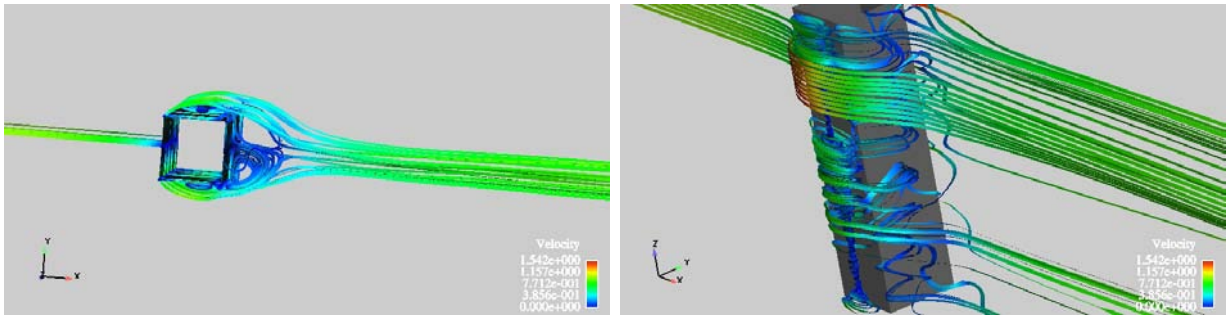


Figure 12: Stream-ribbons from the time-averaged flow, where an exchange of the fluid speed between vortices. Left: an upper-view. Right: a stretching from the lateral to the backward vortices is observed.

face, this picture shows a flow separation.

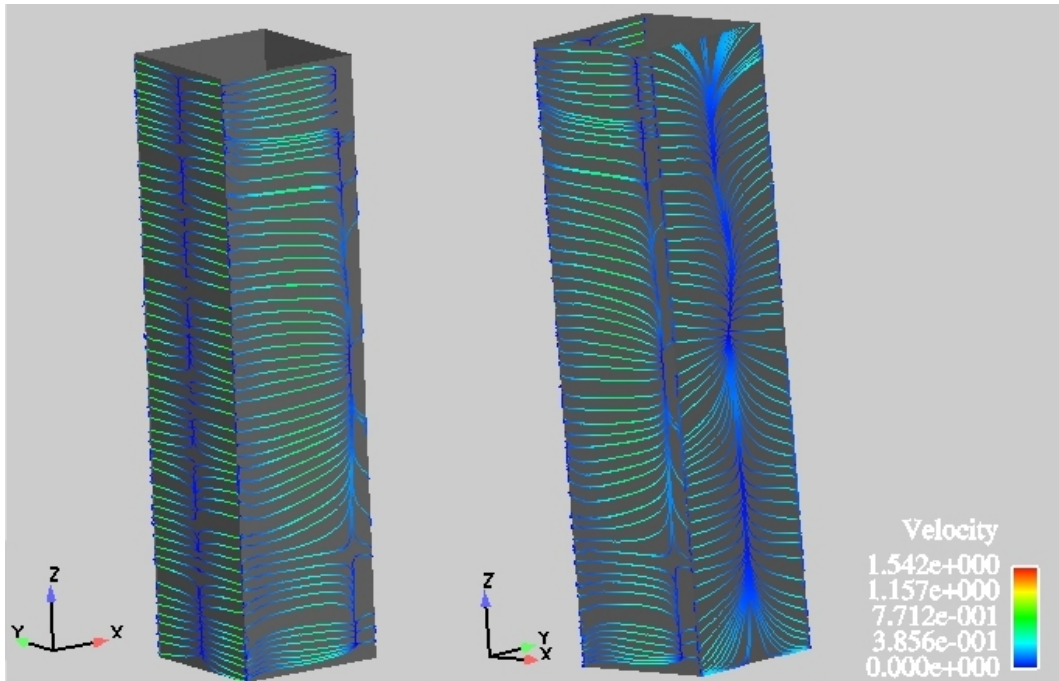


Figure 13: Trace-lines for the time-averaged flow over the body surface: front and lateral sides (left); lateral and rear sides (right).

4.2.6 Isosurfaces of pressure and speed

The isosurface of pressure $p = \pm 0.40 \text{ N/m}^2$ for the time-averaged flow is shown in Fig. 14. It has been found that it is useful for identification of large scale coheren-structures.

Fig. 15 (left) shows the iso-surface of the streamwise velocity of the time-averaged flow for a value $|u| = 0.10 \text{ m/s}$, while Fig. 15 (right) shows the corresponding ones for the speed

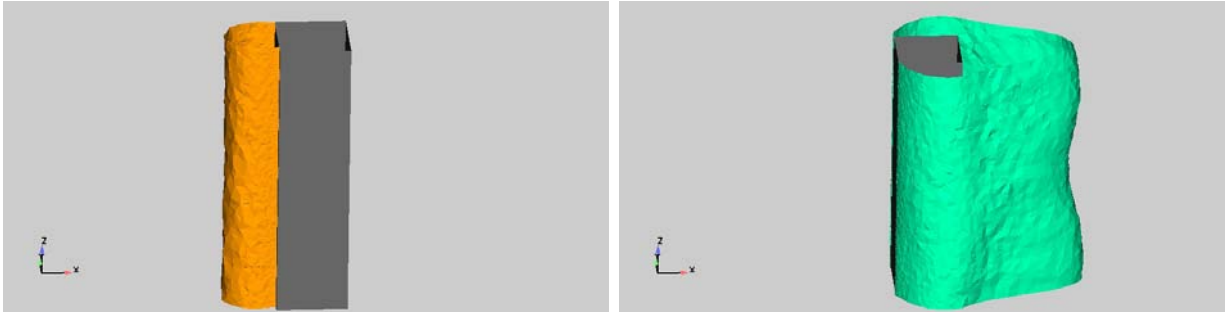


Figure 14: Pressure iso-surfaces for the time-averaged flow: $p = 0.40 \text{ N/m}^2$ (left) and $p = -0.40 \text{ N/m}^2$ (right).

for a value $|v| = 0.50 \text{ m/s}$. Fig.16 plots, on the left, the iso-surfaces of the streamwise velocity $u = 0.40 \text{ m/s}$ of the instantaneous-flow and, on the right, the corresponding ones for the speed for a value $|v| = 0.90 \text{ m/s}$. Both figures show a quasi-periodic flow, with a von Kármán vortex-street in the downstream wake.

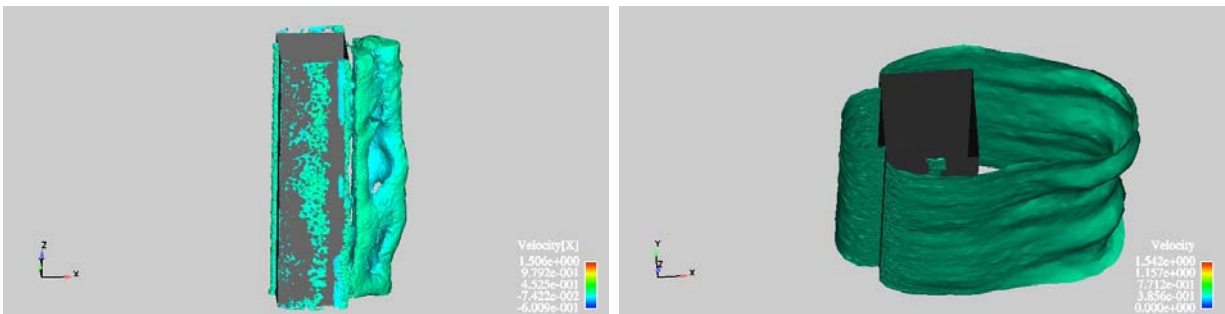


Figure 15: Iso-surfaces from the time-averaged flow for the streamwise velocity $u_x = 0.10 \text{ m/s}$ and for a speed $|v| = 0.50 \text{ m/s}$.

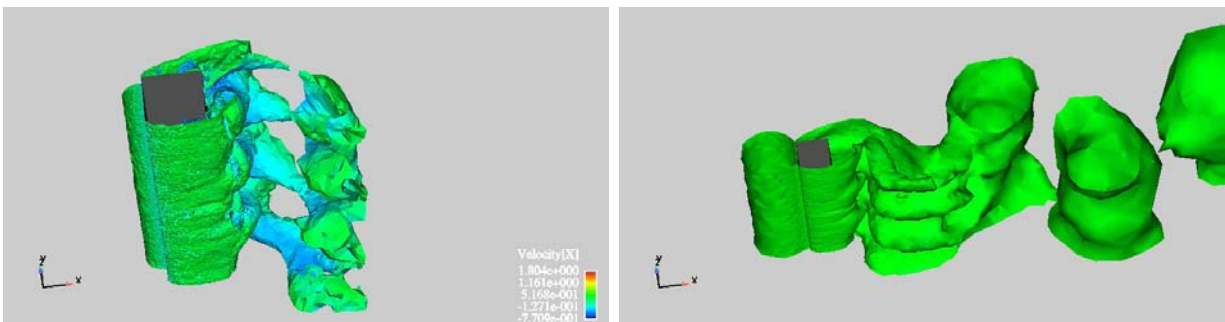


Figure 16: Iso-surfaces from the instantaneous-flow for the streamwise velocity $u_x = 0.40 \text{ m/s}$ and for a speed $|v| = 0.90 \text{ m/s}$.

4.2.7 Contour-fill of speed

The contour-fill of speed are compared in Fig. 17 for the time-average flow and instantaneous one, left and right, respectively, in three horizontal planes. Different topological features can be visualized in each flow, where the iso-surfaces of the instantaneous flow show a periodic behaviour behind the square cylinder.

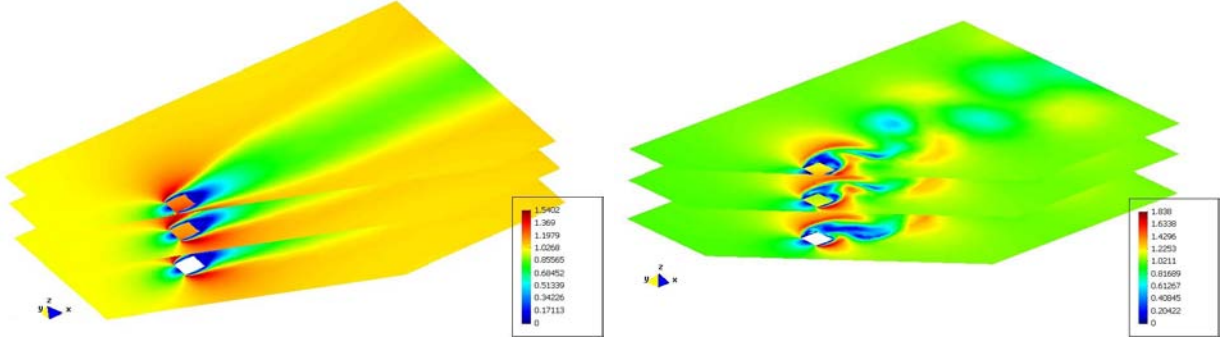


Figure 17: Contour-fill of speed close to the square cylinder: average-flow (left) and instantaneous-one (right).

4.2.8 Isosurfaces of the Q -criterion

For identifying coherent structures, a high vorticity modulus is a possible candidate, especially in free-shear flows, but the technique of iso-surfaces of the Q -criterion can be used to investigate the behaviour in transitional and turbulent flows. So, the so-called Q -criterion is another resource for studies of coherent structures, which often is referred as a $\nabla\mathbf{u}$ -based vortex “eduction method”. It is based on both pressure and vorticity intensities, e.g. see Hunt *et al.*¹⁸, and it can be defined as

$$Q = \frac{1}{2} (\Omega_{ij}\Omega_{ij} - S_{ij}S_{ij}) ; \quad (2)$$

where

$$\begin{aligned} \Omega_{ij} &= \frac{1}{2} \left(\frac{\partial u_i}{\partial x_j} - \frac{\partial u_j}{\partial x_i} \right) ; \\ S_{ij} &= \frac{1}{2} \left(\frac{\partial u_i}{\partial x_j} + \frac{\partial u_j}{\partial x_i} \right) ; \end{aligned} \quad (3)$$

are the symmetrical and skew-symmetrical components of the velocity gradient $\nabla\mathbf{u}$, respectively. In other words, the scalar Q is the second invariant of the velocity gradient $\nabla\mathbf{u}$. From this definition it follows that:

- it is a balance between the squared rotation rate $\Omega^2 = \Omega_{ij}\Omega_{ij}$ and the strain rate $\epsilon(u) = S^2 = S_{ij}S_{ij}$;
- the isosurfaces with $Q > 0$ show sub-flows with rotation rates bigger than the strain ones, so they can be develop coherent structures.

Since $\omega^2 = 2\Omega^2$, another equivalent definition is

$$Q = \frac{1}{4} (\omega^2 - 2S_{ij}S_{ij}) ; \quad (4)$$

showing that the coherent structures have a relatively high concentration of vorticity intensity ω .

Fig. 18, left, shows the isosurfaces $Q > 0$ of the time-average flow for a threshold $[0.2, 0.5]$, where a high vorticity fluctuation is observed in the lateral sides and near-wake, see Figs. 11 and 12, too. The same it is observed with the threshold $[2, 5]$ in Fig. 18, right. Fig. 19 identifying isosurfaces $Q < 0$ to threshold $[-0.2, -0.8]$, where the

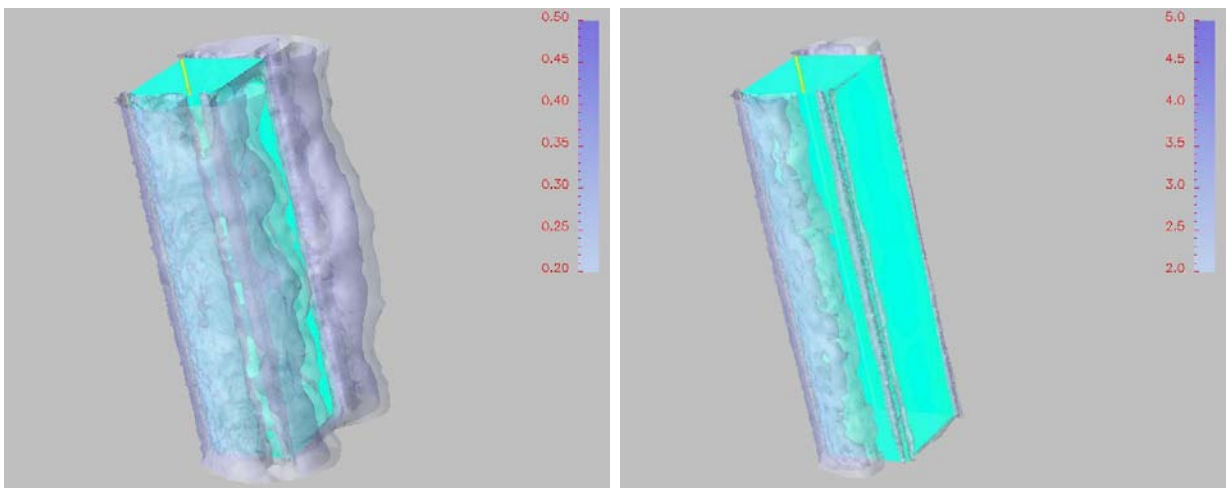


Figure 18: Iso-surfaces $Q > 0$ of the time-averaged flow: for a threshold $[0.2, 0.5]$ (left) and $[2, 5]$ (right).

isosurfaces isolate areas with strain overcomes the strength of rotation. This structures is also observed at the frontal region and center of near-wake, behind the cylinder.

5 CONCLUSIONS

The present work shows flow-visualizations obtained from a LES for the *square cylinder (case A)* proposed in the RE-1995 workshop¹. They reproduce many flow features obtained in other work¹⁹ and observed in laboratory, e.g. see Lyn^{5,6} et al. and Martinuzzi-Tropea⁷, which were detailed in Sec. 4. This bluff-body produces a nearly-periodic flow pattern whose shedding motion is qualitatively well predicted in consonance to the experimental data, while a transition takes place in the separated shear layers on the lateral body sides just downstream of its front corners. On the other hand:

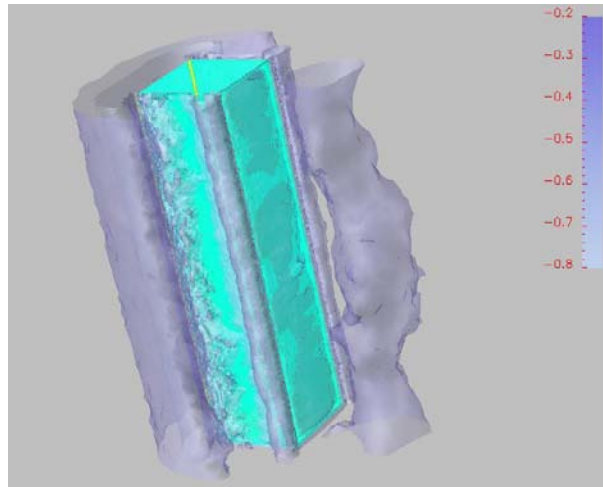


Figure 19: Iso-surfaces of the time-averaged $Q < 0$: threshold $[-0.2, -0.8]$.

- In the RE-1995 workshop¹ it was stressed that numerical simulations based in upwind-like schemes (as the SUPG-PSPG) tend to predict recirculation zones that are shorter than the experimental ones;
- This shortening was attributed (at least partially) to the numerical diffusion that is added by the upwind-like schemes, since it acts as an additional subgrid scale model (to the LES one);
- Due to this drawback, it was recommended that an estimation of the numerical dissipation added by upwind-like schemes should be presented in future benchmarks;
- In the present case, in (unpublished) continuation work of a previous one²⁰, the amount of numerical dissipation introduced in the PETSc-FEM code was estimated around an 18 %. This estimation was obtained through a channel-flow test with a MILES (Monotonically Integrated Large Eddy Simulation, i.e. a LES without a subgrid scale model²¹), where it was verified that the external work was bigger than the dissipation energy (due to the numerical dissipation added by the numerical method), and that the relative difference between external work and dissipation energy was around 18 %.

Acknowledgments

This work was partially performed with the *Free Software Foundation/GNU-Project* resources as GNU/Linux OS and GNU/Octave, as well another Open Source resources as PETSc, MPICH and supported through grants CONICET-PIP-02552/2000, ANPCyT-FONCyT-PME-209 **Cluster**, ANPCyT-FONCyT-PID-99-74 **Flags**, ANPCyT-PICT-6973-BID-1201/OC-AR **Proa** and CAI+D-UNL-2000-43.

REFERENCES

- [1] Rodi W., Ferziger J.H., Breuer M., and Pourquié M. Status of large-eddy simulation: result of a workshop. *ASME transactions*, **119**, 248–262 (June 1997).
- [2] Sagaut P. *Large eddy simulation for incompressible flows, an introduction*. Springer, Berlín, (2001).
- [3] Rodi W. Comparison of les and rans calculation of the flow around bluff bodies. *J. of Wind Engng. and Ind. Aerodyn.*, **69-71**, 55–75 (1997).
- [4] Rodi W. Large-eddy simulations of the flow past bluff bodies. state-of-the art. *Japan Soc. of Mech. Engineers, Int. J.*, **Serie B, vol. 41(2)** (1998).
- [5] Lyn D.A. and Rodi W. The flapping shear layer formed by flow separation from the forward corner of a square cylinder. *J. of Fluid Mechanics*, **267**, 353–376 (1994).
- [6] Lyn D.A., Einav S., Rodi W., and Park J.H. A laser-doppler velocimetry study of ensemble-averaged characteristics of the turbulent near wake of a square cylinder. *J. of Fluid Mechanics*, **304**, 285–319 (1995).
- [7] Martinuzzi R. and Tropea C. The flow around surface-mounted prismatic obstacles placed in a fully developed channel flow. *Journal of Fluids Engineering*, **115**, 85–91 (1993).
- [8] Tezduyar T., Mittal S., Ray S., and Shih R. Incompressible flow computations with stabilized bilinear and linear equal order interpolation velocity-pressure elements. *Comp. Meth. App. Mech. Engng.*, **95(95)**, 221–242 (1992).
- [9] Smagorinsky J. General circulation experiments with the primitive equations: I. the basic equations. *Mon. Weather Rev.*, **91**, 99–164 (1963).
- [10] Sonzogni V.E., Yommi A., Nigro N., and Storti M. A parallel finite element program on a Beowulf Cluster. *Advances in Engineering Software*, **33**, 427–443 (2002).
- [11] D’Elía J., Storti M., Oñate E., and Idelsohn S. A nonlinear panel method in the time domain for seakeeping flow problems. *Int. J. of Computational Fluid Dynamics*, **16(4)**, 263–275 (2002).
- [12] D’Elía J., Storti M., and Idelsohn S. A panel-Fourier method for free surface methods. *ASME-J. of Fluids Engng.*, **122(2)**, 309–317 (June 2000).
- [13] Storti M. and D’Elía J. Added mass of an oscillating hemisphere at very-low and very-high frequencies. *ASME-J. of Fluids Engng.*, **126(6)**, 1048–1053 (November 2005).
- [14] Paz R. and Storti M. An interphase strip precondition for domain decomposition methods. application to hidrology. *Int. J. for Num. Meth. in Engng.*, **62(13)**, 1873–1894 (2005).
- [15] Chong M.S., Perry A.E., and Cantwell B.J. A general classification of three-dimensional flow field. *Phys. Fluids A*, **2**, 765–777 (1990).
- [16] Kenwright D. Automatic detection of open and closed separation and attachment lines. In *Proceedings of IEEE Visualization 98*, (1998).
- [17] Helman J. and Hesselink L. Visualizing vector field topology in fluid flows. In *IEEE*

- Computer Graphics and Applications*, volume 11(3), pages 36–46, (May 1991).
- [18] Hunt J.C.R., Wray A.A., and Moin P. Eddies, stream, and convergence zones in turbulent flows. *Report CTR-S88, Center For Turbulent Research*, (1988).
 - [19] Krajnović S. and Davidson L. Large-eddy simulation of the flow around simplified car model. In *9th Int. Symp. of Flow Visualization*, pages paper 117, 1–10, (2000).
 - [20] D’Elía J., Franck G., Storti M., and Nigro N. Numerical simulations of a fully developed turbulent channel flow by finite elements. In *Mecánica Computacional, vol. XXIII*, pages 2047–2064, (November 08-11 2004).
 - [21] Pope S.B. *Turbulent flows*. Cambridge, 2 edition, (2003).